



Relating Streamer Flows to Density and Magnetic Structures at the Parker Solar Probe

Alexis Rouillard, Athanasios Kouloumvakos, Angelos Vourlidas, Justin Kasper, Stuart Bale, Nour-Edine Raouafi, Benoit Lavraud, Russell Howard, Guillermo Stenborg, Michael H. Stevens, et al.

► To cite this version:

Alexis Rouillard, Athanasios Kouloumvakos, Angelos Vourlidas, Justin Kasper, Stuart Bale, et al.. Relating Streamer Flows to Density and Magnetic Structures at the Parker Solar Probe. The Astrophysical Journal Supplement, 2020, 246 (2), pp.37. 10.3847/1538-4365/ab579a . hal-02886381

HAL Id: hal-02886381

<https://hal.science/hal-02886381>

Submitted on 2 Jul 2020

HAL is a multi-disciplinary open access archive for the deposit and dissemination of scientific research documents, whether they are published or not. The documents may come from teaching and research institutions in France or abroad, or from public or private research centers.

L'archive ouverte pluridisciplinaire **HAL**, est destinée au dépôt et à la diffusion de documents scientifiques de niveau recherche, publiés ou non, émanant des établissements d'enseignement et de recherche français ou étrangers, des laboratoires publics ou privés.



Distributed under a Creative Commons Attribution - NonCommercial 4.0 International License



Relating Streamer Flows to Density and Magnetic Structures at the *Parker Solar Probe*

Alexis P. Rouillard¹ , Athanasios Kouloumvakos¹, Angelos Vourlidas² , Justin Kasper^{3,4} , Stuart Bale^{5,6,7,8} ,
 Nour-Edine Raouafi², Benoit Lavraud¹ , Russell A. Howard⁹ , Guillermo Stenborg⁹ , Michael Stevens⁴ , Nicolas Poirier¹ ,
 Jackie A. Davies¹⁰, Phillip Hess⁹, Aleida K. Higginson² , Michael Lavarra¹, Nicholeen M. Viall¹¹ , Kelly Korreck⁴ ,
 Rui F. Pinto¹ , Léa Griton¹, Victor Réville¹ , Philippe Louarn¹, Yihong Wu¹, Kévin Dalmasse¹ , Vincent Génot¹,
 Anthony W. Case⁴ , Phyllis Whittlesey⁶, Davin Larson⁶, Jasper S. Halekas¹² , Roberto Livi¹³, Keith Goetz¹⁴, Peter R. Harvey⁶,
 Robert J. MacDowall¹⁵ , D. Malaspina¹⁶ , M. Pulupa⁶ , J. Bonnell⁶, T. Dudok de Witt¹⁷ , and Emmanuel Penou¹

¹IRAP, Université Toulouse III—Paul Sabatier, CNRS, CNES, Toulouse, France; arouillard@irap.omp.eu

²Johns Hopkins University Applied Physics Laboratory, Laurel, MD 20723, USA

³Climate and Space Sciences and Engineering, University of Michigan, Ann Arbor, MI 48109, USA

⁴Smithsonian Astrophysical Observatory, Cambridge, MA 02138 USA

⁵Physics Department, University of California, Berkeley, CA 94720-7300, USA

⁶Space Sciences Laboratory, University of California, Berkeley, CA 94720-7450, USA

⁷The Blackett Laboratory, Imperial College London, London, SW7 2AZ, UK

⁸School of Physics and Astronomy, Queen Mary University of London, London E1 4NS, UK

⁹Naval Research Laboratory, Washington, DC, USA

¹⁰RAL Space, STFC-Rutherford Appleton Laboratory, Didcot, UK

¹¹Heliophysics Division, NASA Goddard Space Flight Center, Greenbelt, MD 20771, USA

¹²Department of Physics and Astronomy, University of Iowa, IA 52242, USA

¹³University of California, Space Science Laboratory, Berkeley, CA, USA

¹⁴School of Physics and Astronomy, University of Minnesota, Minneapolis, MN 55455, USA

¹⁵NASA Goddard Space Flight Center, Greenbelt, MD, USA

¹⁶University of Colorado, Boulder, Laboratory for Atmospheric and Space Physics, Boulder, CO, USA

¹⁷LPC2E, CNRS and University of Orléans, Orléans, France

Received 2019 September 15; revised 2019 November 1; accepted 2019 November 7; published 2020 February 3

Abstract

The physical mechanisms that produce the slow solar wind are still highly debated. *Parker Solar Probe*'s (*PSP*'s) second solar encounter provided a new opportunity to relate in situ measurements of the nascent slow solar wind with white-light images of streamer flows. We exploit data taken by the *Solar and Heliospheric Observatory*, the *Solar Terrestrial Relations Observatory* (*STEREO*), and the Wide Imager on *Solar Probe* to reveal for the first time a close link between imaged streamer flows and the high-density plasma measured by the Solar Wind Electrons Alphas and Protons (SWEAP) experiment. We identify different types of slow winds measured by *PSP* that we relate to the spacecraft's magnetic connectivity (or not) to streamer flows. SWEAP measured high-density and highly variable plasma when *PSP* was well connected to streamers but more tenuous wind with much weaker density variations when it exited streamer flows. *STEREO* imaging of the release and propagation of small transients from the Sun to *PSP* reveals that the spacecraft was continually impacted by the southern edge of streamer transients. The impact of specific density structures is marked by a higher occurrence of magnetic field reversals measured by the *FIELDS* magnetometers. Magnetic reversals are associated with much stronger density variations inside than outside streamer flows. We tentatively interpret these findings in terms of magnetic reconnection between open magnetic fields and coronal loops with different properties, providing support for the formation of a subset of the slow wind by magnetic reconnection.

Unified Astronomy Thesaurus concepts: Slow solar wind (1873); Solar coronal streamers (1486); Solar coronal transients (312)

1. Introduction

The solar wind plasma measured in situ has been classified into several different categories that could be related to different coronal sources (e.g., Xu & Borovsky 2015). The most clearly identified source regions visible in extreme ultraviolet (EUV) observations of the low corona are coronal holes. They host the footpoints of magnetic field lines connecting the corona to the interplanetary medium (e.g., Krieger et al. 1973; Bame et al. 1976; Levine et al. 1977).

There is currently no doubt that the fast and more tenuous solar wind originates in these coronal holes.

In contrast, the origin of the slow solar wind is less well understood. It could form by a number of distinct processes and from a number of different coronal structures including (1) the boundary of polar coronal holes and isolated low-latitude coronal holes (e.g., Wang 1994) and (2) small patches of open magnetic fields rooted in the vicinity of the magnetic loop complexes of active regions (e.g., Kojima et al. 1999; van Driel-Gesztelyi et al. 2012; Culhane et al. 2014). The slowest and densest solar wind measured in situ can be traced back to regions of the corona, called streamers, that appear very bright in white-light images (Sanchez-Diaz et al. 2016, 2017a). Coronal rays are narrow lanes of enhanced brightness that extend from the corona to several tens of solar radii



Original content from this work may be used under the terms of the [Creative Commons Attribution 4.0 licence](https://creativecommons.org/licenses/by/4.0/). Any further distribution of this work must maintain attribution to the author(s) and the title of the work, journal citation and DOI.

(Druckmüller et al. 2014). Coronal rays are referred to as streamer rays when they originate in the vicinity of either helmet streamers or pseudo-streamers. Helmet streamers are systems of magnetic loops that separate open magnetic field lines of opposite magnetic polarity. The plasma escaping along these open magnetic field lines forms the helmet streamer rays. The polarity inversion line or coronal neutral line that forms near the tip of helmet streamers is the coronal origin of the heliospheric current sheet (HCS). Helmet streamer rays are thought to engulf the HCS and be the source of the heliospheric plasma sheet (HPS) typically measured in situ during crossings of the HCS (Winterhalter et al. 1994). Pseudo-streamers are coronal structures that separate open magnetic field lines of the same polarity; they produce streamer rays but do not produce a current sheet in the outer corona (Wang et al. 2007).

The plasma outflows imaged along helmet streamer rays is highly intermittent and can be highly variable. A subset, at least, of these transient structures has been interpreted as outflowing magnetic flux ropes based on the analysis of multipoint imagery (Sheeley et al. 2009) and the continuous tracking of these structures to their in situ counterparts (Rouillard et al. 2009, 2010a, 2010b, 2011). Smaller scale density fluctuations detected in situ (Viall et al. 2008) in the slow wind have also been seen adjacent to small flux ropes (Kepko et al. 2016) and have been related to brightness variations in the corona (Viall & Vourlidas 2015). There is no doubt that a significant subset of the slow solar wind is composed of transient structures that form in the corona, many near the tip of helmet streamers where magnetic reconnection must occur, due to the presence of current sheets and null points (Sanchez-Diaz et al. 2017a, 2017b).

However, the slow solar wind appears to originate from a very broad region of the corona, extending up to 40° – 50° away from the coronal neutral line. This suggests that the coronal conditions that produce the slow solar wind do not depend on the presence of a polarity inversion line. Background solar wind models that assume a coronal heating rate dependent on the local magnetic field properties lead to the interpretation that the slow solar wind is a natural consequence of the expansion rate of open magnetic field lines that channel the wind (e.g., Linker et al. 1999; van der Holst et al. 2010; Pinto & Rouillard 2017). The dependence of heating rates on the magnetic field properties find their justification in more detailed coronal heating models driven by Alfvén waves. None of these models are yet capable of simulating the composition of the slow solar wind, which would require a more dynamic mechanism involving reconnection between open and closed magnetic field lines (e.g., Baker et al. 2009).

As already stated, the densest and slowest wind is traced back to the coronal neutral line where the bright streamer rays are formed. The thickness of these streamer rays can be measured in white-light images when the streamer is observed edge on. They typically extend over 10° – 20° in heliocentric latitude. Such a measurement represents a maximum thickness because even small latitudinal changes of the streamer belt would artificially broaden this region due to line-of-sight effects. This effect is analyzed using the Wide-field Imager for Solar PRobe (WISPR) data by Poirier et al. (2020) and also in the present paper. This angular extent is naturally much broader than that of the very thin and unresolved current sheet embedded in these coronal rays. The in situ counterparts of the coronal neutral line and the streamer rays are thought to be the HCS and the dense HPS. The HCS extends in situ over a heliocentric radial distance of just 1–10 Mm while the HPS is

about 500–700 Mm (Winterhalter et al. 1994), which is on the upper end of the observed latitudinal extent of streamer rays, 10° – 20° , when observed near $3 R_{\odot}$.

Synthetic white-light images produced by three-dimensional (3D) coronal models provide a good representation of the extent of streamer rays and therefore the HPS (e.g., Pinto & Rouillard 2017; Poirier et al. 2020). In such simulations, the dense coronal regions result from the properties of magnetic field lines that are directly adjacent to the helmet streamer. Strong heating at the base of flux tubes, associated with strong footpoint field strengths, drives a high mass flux into the wind. In addition, the large expansion rate of flux tubes forces a rapid drop in the heating rate with altitude, preventing a strong acceleration of a dense wind (e.g., Wang 1994; Pinto & Rouillard 2017). The excess density observed around the current sheet is related to a reconvergence of flux tubes near the top of helmet streamers. This produces a very slow and dense wind along the rays extending above streamer tops, which forms the HPS (e.g., Wang 1994; Pinto & Rouillard 2017).

In addition to the intermittent eruption of helical magnetic fields already identified along streamer rays (Rouillard et al. 2009, 2010a, 2010b, 2011) and the continuous outflow of a very dense and slow background solar wind (e.g., Pinto & Rouillard 2017), we expect other dynamic processes to perturb the solar wind from streamers. These include magnetic reconnection between coronal loops and open magnetic fields that connect to the streamer tops or, instead, between open magnetic field lines of opposite polarities that meet at the streamer tops. This should produce transient outflows with distinct magnetic signatures and shears that would modify the properties of the wind expelled from streamer rays (e.g., Owens et al. 2018).

Due to the large distances between the regions imaged by coronagraphs and in situ measurements taken mostly near 1 au (astronomical unit), streamer flows that fade by 60–70 solar radii could not be related clearly with in situ measurements until now. Previous analyses based on heliospheric imaging were limited to tracking only those streamer transients from the corona to 1 au that become swept up by high-speed streams. The advent of *PSP* and its measurements of the background solar wind as close as 35 solar radii (Bale et al. 2019; Kasper et al. 2019/this volume) alleviate some of these past difficulties. Even white-light features that disappear by 50–70 solar radii in heliospheric images (Eyles et al. 2009) taken by *STEREO* can be detected by the *PSP* plasma and magnetic field detectors before they are no longer discernible in the images. In the present paper, we exploit multipoint data during *PSP*'s second solar encounter. At this time, *STEREO-A* (*STA*) was optimally located to track density variations continuously from the Sun to *PSP*.

The present work is structured as follows. We start by presenting the observational context from both a remote-sensing and in situ perspective. We then present the *Solar and Heliospheric Observatory* (*SOHO*), *STEREO*, and *PSP* images of bright structures expelled by helmet streamers in the direction of *PSP*. In the third part, we compare these images with the in situ measurements from *PSP* at the predicted times of impact of the imaged density structures and reveal the presence of multiple switchbacks. Finally, we discuss the possible origins of these features at the Sun by considering *STEREO* EUV images.

2. Orbital Details of the Second *PSP* Encounter

The second *PSP* solar encounter occurred between 2019 March 30 and 2019 April 10. Figure 1 presents views of the ecliptic

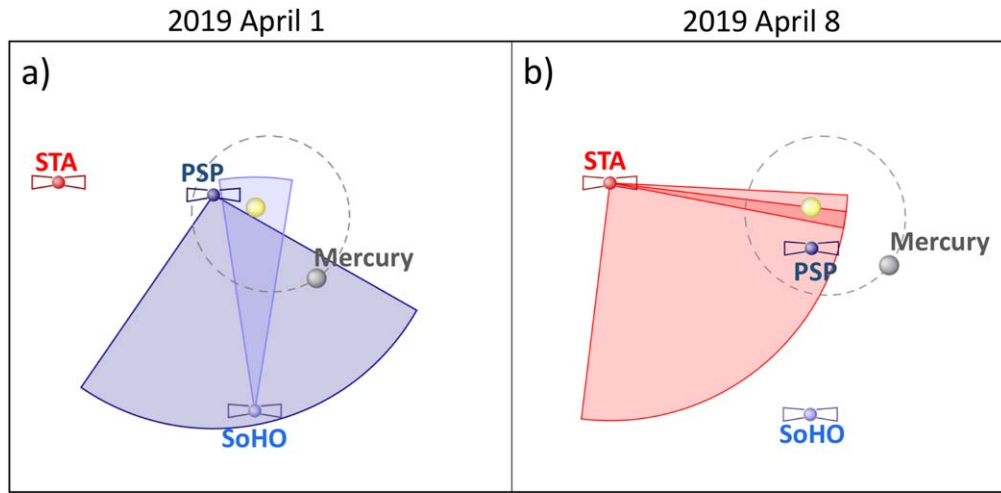


Figure 1. Two views of the ecliptic plane from solar north showing the orbital positions of *STA*, *PSP*, and *SOHO* in inertial coordinates (Heliocentric Aries Ecliptic) on 2019 April 1 and 8. The fields of view of the combined *PSP* WISPR, *SOHO* LASCO C3, and *STA* COR2/HI1 instruments used in this study are shown as dark blue, light blue, and red shaded areas, respectively. The position of Mercury is also shown as a gray disk. This figure was produced using the Propagation Tool described in Rouillard et al. (2017).

plane from solar north, inside this time window, on April 1 and 8. The figure also shows the combined fields of view of the WISPR (Vourlidis et al. 2016) instruments on *PSP* (shown as a shaded blue area), *SOHO* LASCO C3 instrument (Brueckner et al. 1995) as well as the Outer CORonagraph (COR2) and the combined Heliospheric Imagers (HI1 and HI2) instruments (red shaded areas) on board *STA*. The latter instruments form part of the Sun-Earth Connection Coronal and Heliospheric Investigation (SECCHI) package (Howard et al. 2008).

PSP is located off the east limb of the Sun just outside the outer edge of the *SOHO* C3 field of view. On April 8, *PSP* was situated inside the field of view of the *STA* HIs that were imaging plasma off the west limb of the Sun viewed from *STA*. Plasma that escaped the Sun could have been imaged by SECCHI before it was measured in situ by *PSP*.

We can illustrate this observational capability in more detail by changing from an inertial to a Sun-corotating frame such as Carrington coordinates. This representation is shown in Figure 2 for the time interval of interest here. The theory of Thomson scattering tells us that coronal regions located near the “Thomson sphere” contribute most to the visible light recorded by an imager (Vourlidis & Howard 2006). Figure 2 illustrates the total ecliptic area observed by the section of the Thomson sphere inside the field of view of the *STA* (COR2/HI1) and WISPR-I instruments of *PSP* and *STA* from 2019 April 5 to 10. The WISPR instruments consist of two cameras, in the inner (WISPR-I) and outer (WISPR-O) imagers; in this study, we make use of WISPR-I. WISPR-I extends in elongation angles from 13.5° to 53° and WISPR-O extends from 50° to 108° .

Figure 2 also shows that *PSP*’s orbit remained near the Thomson sphere of *STA* for an extended period from April 6 to 9. The Carrington longitude of *PSP* only changed by 4.5° between April 5 and 11, moving from 7.6° to 12.1° longitude, respectively. *PSP* was making in situ measurements in almost the same region during the period we focus on here.

3. Relating Streamer Rays to the Dense Solar Wind

To provide further context to the analysis that follows, we present in Figure 3(a) a Carrington map obtained from LASCO

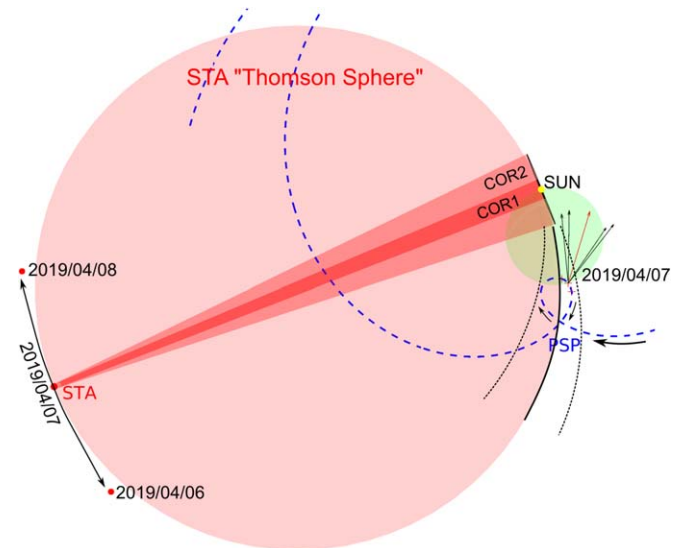


Figure 2. View of the ecliptic plane from solar north showing the relative positions of the Sun, *STA* (red), and *PSP* (blue) in Carrington coordinates on 2019 April 7. In this coordinate system, the orbit of *PSP*, shown as a dashed blue line, executes a loop near perihelion. The Thomson sphere of *STA* is shown as the red disk and that of *PSP* as a green disk. The fields of view of *STA* COR1 and COR2 depicted with different shades of red and the area swept by the extent of the field of view of HI1 can be seen as the black curve on *STA*’s Thomson sphere. This curve sweeps an area bound by two similar black dotted curves between April 6 and April 8, the time interval when ejections are analyzed in this paper. These black dotted curves bound the entire perihelion passage, meaning that density structures can be tracked near the Thomson sphere of *STA* continuously from the Sun to *PSP* at these times.

C3 observations on board *SOHO* during a whole solar rotation. This Carrington map is constructed by taking a band of pixels at a given heliocentric radial distance from each LASCO C3 image to produce a latitudinal strip. Each strip is then assigned a Carrington longitude by assuming that the observed brightness comes from the Thomson sphere of the instrument. This representation provides a powerful way of visualizing the global structure of the streamers. The bright band observed at low latitude and near the equator, and extending over all longitudes, is the streamer belt that corresponds to the densest

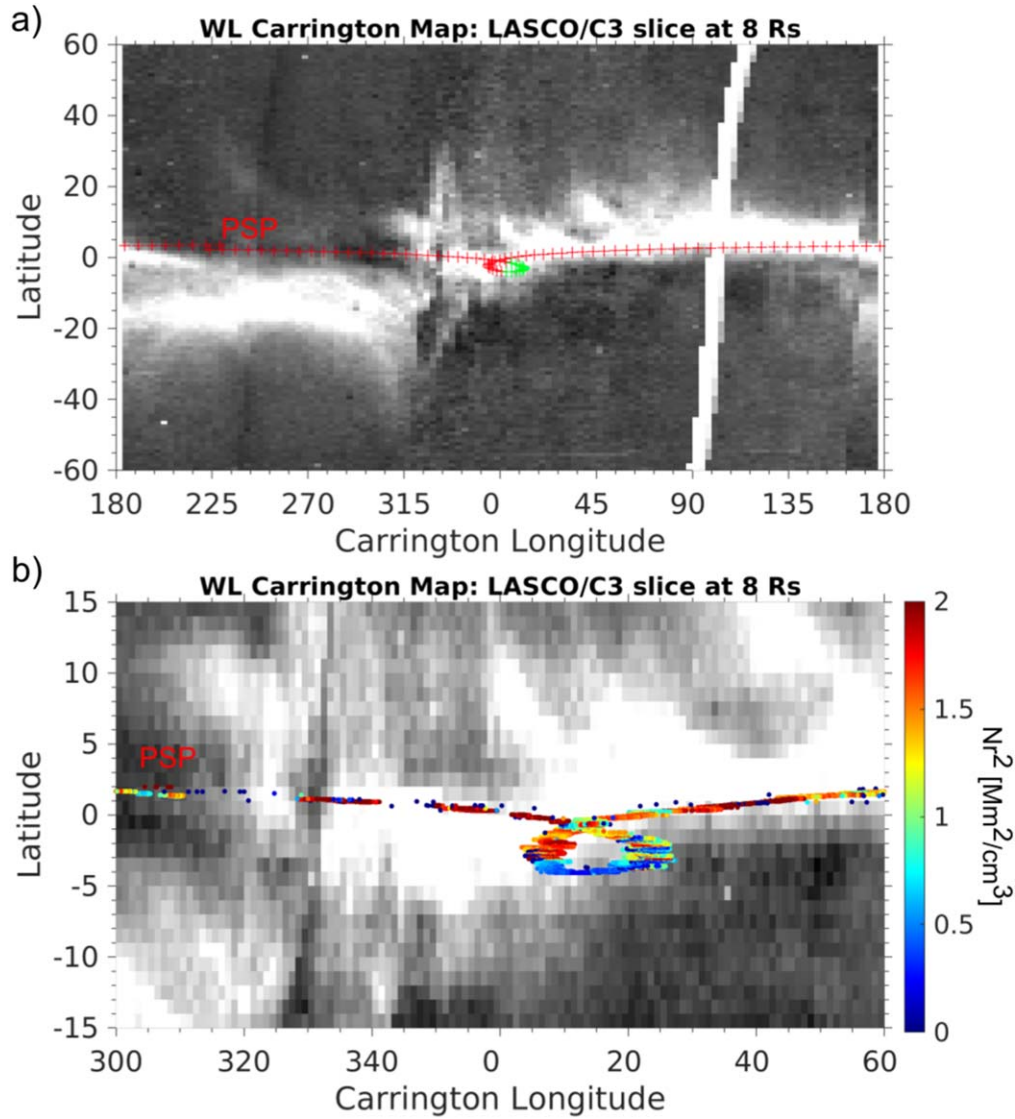


Figure 3. Comparison of the relative heliographic positions of *PSP* and streamer rays at $8 R_{\odot}$. Panel (a): a full Carrington map constructed by extracting pixels of LASCO C3 images along the arc of a circle centered at the Sun center and passing at $8 R_{\odot}$ off the east solar limb as viewed from *SOHO*. The heliographic coordinates of *PSP* (without accounting for propagation effects) is shown as the red crosses. The part of the orbit that we focus on here is highlighted with green crosses. Panel (b): a zoomed-in view of the same Carrington map but focusing on the encounter period. The *PSP* path corresponds to the points of magnetic connectivity traced back to the radial distance of the map ($8 R_{\odot}$). The connectivity is estimated by assuming the magnetic field follows a Parker spiral calculated from the speed of the solar wind measured in situ at *PSP*. The color coding is defined by the density (Nr^2) measured in situ by *PSP* with red corresponding to high densities and blue to low densities.

regions of the corona. As discussed in the introduction, the latitudinal width of the band is about 10° – 20° .

The trajectory of *PSP* is overplotted as red/green crosses on this map. The periods of corotation and superrotation can be seen as the small loop near Carrington longitudes 355° – 10° (near the center of the map). The map reveals that *PSP* remained near the edge of the streamer belt throughout its second encounter. As *PSP* did not cross the center of the streamer until well after perihelion, we expect from Figure 3 that the probe remained in the same magnetic sector for most of the second encounter. In situ measurements of the magnetic field confirm that *PSP* only crossed the polarity inversion line on around April 16, well after perihelion.

We present in Figure 4 a summary plot of in situ measurements made by *PSP* over a 10 day period centered on perihelion. The *FIELDS* suite of instruments provided combined measurements of magnetic and electric fields (Bale et al. 2016). Magnetic fields are measured using both fluxgate

and search-coil (induction) magnetometers mounted on a deployable boom in the spacecraft umbra. We here show measurements made by the magnetometer. As highlighted in Bale et al. (2019), the *FIELDS* magnetometer measured magnetic fields with predominantly Sun-pointing polarity throughout the second encounter. This is reflected in panel (a), where the radial field component remains negative. As discussed by Bale et al. (2019) and Kasper et al. (2019), the magnetic field exhibited sudden short-lived reversals of the magnetic field direction that were not associated with correlated changes in the pitch angle of suprathermal electrons. Hence, the polarity of magnetic fields does not change in these structures, and the reversals are interpreted as “folds” or “switchbacks” in the magnetic field lines (Bale et al. 2019). These are clearly seen in panel (a). We plot here the radial magnetic field multiplied by the square of the heliocentric radial distance of the spacecraft ($B_r r^2$) to remove the effect of the varying heliocentric distance of the spacecraft.

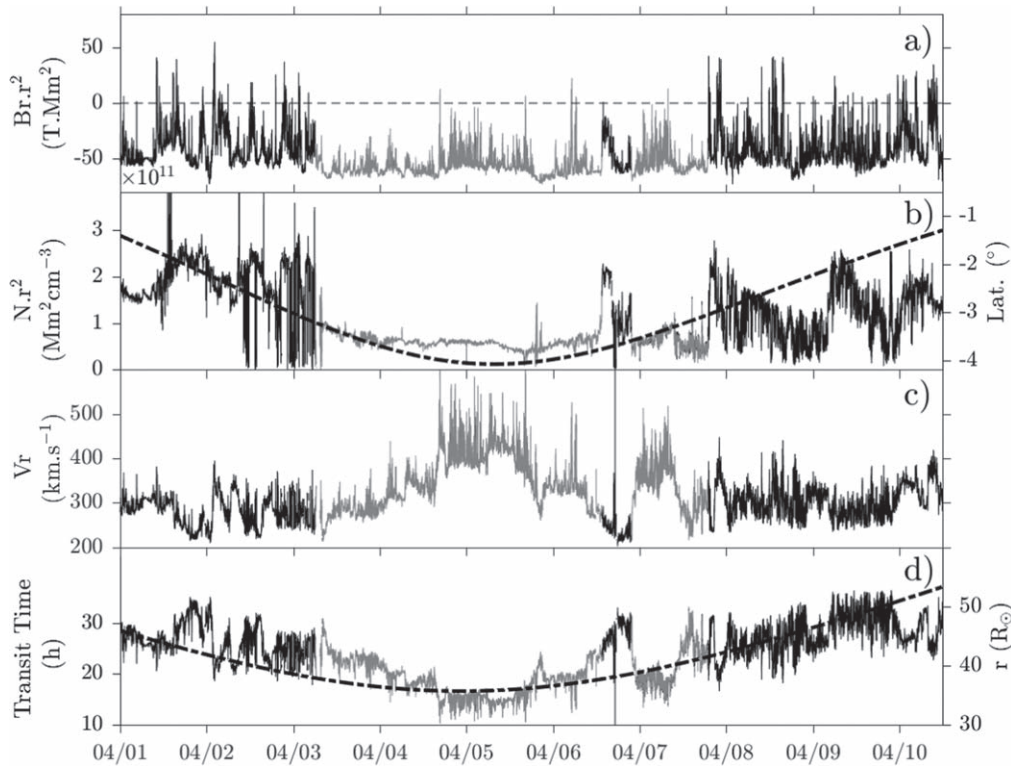


Figure 4. In situ measurements taken by the FIELDS and SWEAP instrument suites on *PSP* over a 10 day interval centered around *PSP*’s second perihelion. Panel (a): the measured radial component of the magnetic field (B_r) in radial tangential normal (RTN) coordinates, multiplied by the square of the radial distance (r^2). Panel (b): proton density of the solar wind (N) also multiplied by r^2 . The heliographic latitude (Lat. ($^\circ$)) of *PSP* is also plotted as a dashed–dotted line. Panel (c): the radial speed of solar wind protons (V_r). Panel (d): the plasma transit time from the $2.5 R_\odot$ to *PSP* in hours (hr) computed from V_r . The heliocentric radial distance of *PSP* is also shown as a dashed–dotted line. The plasma measurements associated with streamer flows in this study are shown in black while those from outside streamers are shown in gray. The in situ data were averaged over 30 s.

The density and speed of the solar wind protons are measured by the Solar Probe Cup (SPC) part of the instrument suite of the Solar Wind Electrons Alphas and Protons (SWEAP; Kasper et al. 2016) experiment. The Solar Probe Cup has a 60° Sun-pointing (full-width) field of view and is placed near the edge of the probe’s heat shield. The operating principle of the instrument is described in Case et al. (2020) and is similar to that of previous Faraday Cup experiments in space. The instrument measures the current deposited by inflowing ions (or electrons) onto a segmented metal plate at the base of the cup, and those charge carriers are discriminated with respect to their kinetic energy per charge using a set of transparent, high-voltage grids to which an A/C waveform is applied. The A/C waveform is stepped through a series of subranges in voltage spanning the energy of the bulk solar wind, and the corresponding amplitudes of the modulated current are used to reconstruct the radial kinetic energy-per-charge distribution function for the solar wind. The proton density, temperature, and velocity moments are derived from direct integration of the measured distribution in the neighborhood of the primary peak in the ion current (Case et al. 2020). The 30 s averages of proton densities and radial speeds derived from SPC data are shown in panels (b) and (c) of Figure 4. The proton densities have been multiplied by r^2 in panel (b). Like the magnetic field data, the proton densities also display considerable variability. The SPC appears to have measured different regimes of solar wind during the encounter, with periods of dense, highly variable, and very slow solar wind ($\leq 300 \text{ km s}^{-1}$) and less dense and faster plasma ($> 300 \text{ km s}^{-1}$) close to perihelion. We have used different shades of black and

gray on this panel to highlight these different regimes. We also overplot in panel (b) the rapidly changing heliographic latitude of the spacecraft. We interpret these three regimes as a consequence of the changing latitude of *PSP*, which temporarily exits the streamer flows.

To test this idea, Figure 3(b) provides a zoomed-in view of panel (a) around perihelion. In Figure 3(b), we trace back the magnetic connectivity of *PSP* to the height at which the map is constructed, e.g., $8 R_\odot$, by using the solar wind speed measured in situ by *PSP* (see Figure 4(c)). *PSP*’s movement of a few degrees in latitude is clearly seen in this zoomed-in view (Figure 3(b)). The map reveals that *PSP* temporarily moved away from the center of the streamer into a less bright region before rapidly re-entering the streamer. To compare directly the brightness in our map with the measured plasma densities, we have color-coded the trajectory of *PSP* according to the density (Nr^2) measured in situ. We can clearly see that the elevated density measured by *PSP* corresponds to periods when the spacecraft is connected to the streamer flows. The lowest plasma density corresponds to periods when *PSP* exits the streamer temporarily. Such a close match between plasma flows measured in situ and coronal images is unprecedented and is, of course, related to the proximity of *PSP* to the corona, with the spacecraft only about $20 R_\odot$ away from the imaged streamer rays.

Figure 5 presents a similar map but constructed using WISPR-I images taken between April 1 and 8. WISPR-I is a white-light instrument that observes and records the brightness of the F-corona, produced by light scattered off dust (Stenborg et al. 2018), and the K-corona, produced from the scattering of

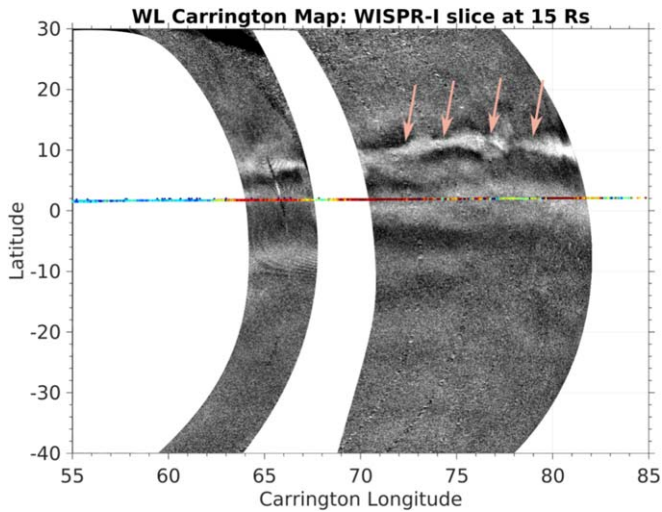


Figure 5. Similar to Figure 3 but for WISPR-I observations and limited to the range of Carrington longitudes imaged by WISPR-I (between 55° and 85°). The colored line indicates the heliographic coordinates at the radial distance of the map ($15 R_\odot$) of the Parker spiral connected to *PSP*. Its color coding is defined by the normalized density (Nr^2) measured in situ by *PSP* with red corresponding to high densities and blue to low densities. The colored arrows mark the likely location of the coronal neutral line.

photospheric light by coronal and solar wind electrons. The Level-1 FITS files contain brightness measurements that must be normalized for exposure time and then corrected for the vignetting effects of the detector. The vignetting function and calibration constant were both initially determined during preflight calibration of the instrument but have since been modified based on stellar photometry using techniques adapted from Bewsher et al. (2012) and Tappin et al. (2015). The signal of the F-corona was removed by adapting a technique developed by Stenborg et al. (2018) on SECCHI H11 data. This technique was applied to all WISPR-I data to produce images of the K-corona. The technique used to build the Carrington map from WISPR-I images is described in detail in Poirier et al. (2020). A search is made in each image of the K-corona for all pixels associated with lines of sight intersecting the Thomson sphere at a heliocentric radial distance of $15 R_\odot$. As highlighted by Figure 2, WISPR-I provides a zoomed-in view of the corona. The WISPR-I data in Figure 5 cover a small range of Carrington longitudes from 55° to 85° . The bright band of pixels that we associated with streamer rays in the LASCO C3 Carrington map extended from $\sim -5^\circ$ to about 10° between Carrington longitudes 40° and 80° ; this matches the latitudinal band where we see the brightest rays in the WISPR-I map in Figure 5. Similar to the maps produced for the first encounter and analyzed in detail by Poirier et al. (2019, this volume), the WISPR-I images reveal substructure in the streamer rays that is not visible in LASCO (Figure 3) or *STEREO* images. The plasma imaged by WISPR-I over the range of longitudes shown in Figure 5 is related to source regions that released plasma toward *PSP* between March 23 and 27, well before the start of the second encounter. Hence, we cannot make the one-to-one association between WISPR-I imagery and *PSP* in situ data; in contrast, this is possible with *STA* images, as shown later in this paper.

We plot on this map the normalized density (Nr^2) measured in situ by *PSP* with the same color scheme as in Figure 3. The plasma densities are very elevated during this time interval because the probe is passing near the southern edge of the streamer flows. The brightest rays marked by arrows in this map correspond to the densest part of the streamer, where the

current sheet is likely to be located. If this is the case, then Figure 5 reveals that *PSP* passed just 4° – 10° south of the HCS during this time. The in situ measurements confirm that *PSP* remained in the negative polarity during this time interval and did not cross the HCS (Bale et al. 2019/this volume). The flows are perturbed by bursts of switchbacks.

We conclude from these preliminary studies that *PSP* primarily sampled plasma escaping from the southern flank of the streamer; therefore, the probe remained in a single magnetic sector (inward-pointing magnetic fields) throughout the second encounter and, in particular, during the period of interest here. The plasma density normalized by r^2 inside the streamer flows is up to a factor of 6 higher than that in the slow wind emerging outside streamers. Near perihelion, *PSP* temporarily exited the streamer to sample more tenuous slow solar wind emerging from another source that could be associated with a region just inside the outer edge of a coronal hole. We find evidence that the reversals of the magnetic field lines detected by FIELDS occur in bursts or clumps when they originate in streamer flows, and are sometimes accompanied by significant density variations. The densest plasma measured by SPC exhibits great variability, with changes of normalized density of a factor of 3; such fluctuations should easily be detected as strong brightness variations by coronagraphs and heliospheric imagers. In contrast, the switchbacks that occur in the slightly faster and more tenuous solar wind outside streamer flows are shorter lived and do not exhibit strong density variations. These should remain undetected in current white-light instruments.

We now investigate the origin of the density structures detected by *PSP* between April 6 and 11 as it re-entered streamer flows, by using multipoint coronal imaging. This period is of great interest because, as already stated, the plasma directed toward *PSP* should have been imaged by *STA*.

4. Streamer Activity Captured by *STEREO-A*

We begin this section by examining coronal activity off the west limb of the Sun imaged by *STA* COR2 and H11. Figure 6(a) shows a COR2 image from 2019 April 6 00:24 UT where we have subtracted the background F-corona to reveal the K-corona. This image shows the presence of a streamer located a few degrees north of the equatorial plane and bright rays that start to appear just a few degrees south of that streamer. At these times, the position angle (PA) of *PSP* lies along the southern rays, south of the main streamer rays in this image. This is expected from examination of Figure 3(b) because, just after perihelion (right-hand side of the loop at 20° Carrington longitude), *PSP* is located just south of the bright streamer and west of the portion of a streamer that is entering the plane of the sky of *STA*.

In panels (b)–(e) of Figure 6, we present four COR2A running-difference images from the period April 6 to 9, at times when small-scale transient structures were ejected over the west solar limb. Red arrows in those panels mark those ejecting dense structures (so-called “blobs”). Some of the structures take the shapes of loops; others have V-shaped aspects. They are reminiscent of the ejection of helical magnetic fields (Sheeley et al. 2009).

Most of the streamer outflows could be traced into H11 images, and a subset as far out as H12. Figure 7 presents two H11 running-difference images that show some of the streamer outflows. Based on the *PSP* orbit shown in Figure 2, H11

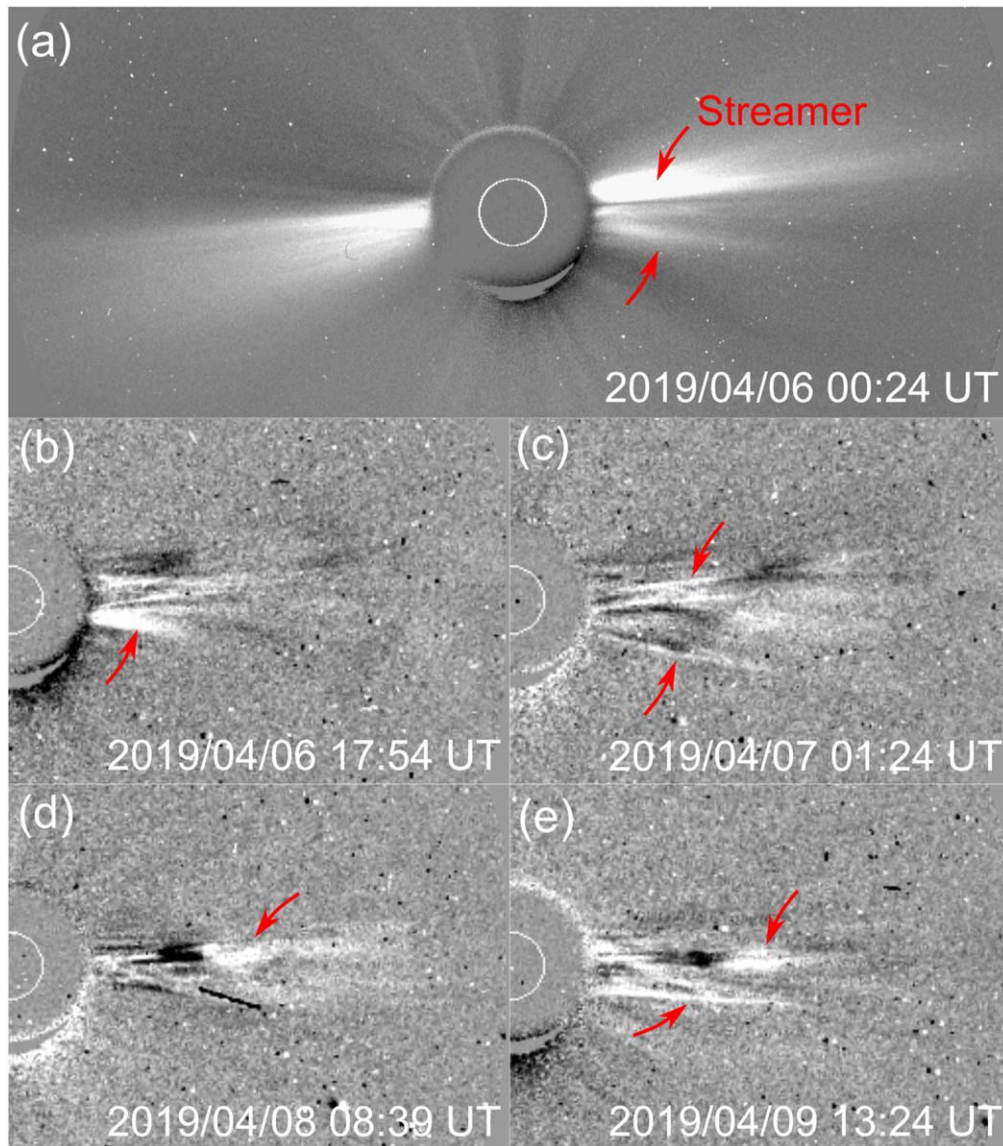


Figure 6. Panel (a): a background-subtracted COR2A image from April 6, just after *PSP*'s perihelion. We label the position of the bright west-limb streamer in red and mark additional streamer rays that suddenly appear in the image. Panels (b)–(e): running-difference images from COR2A throughout the time interval extending from April 6 to 9, during which we track density structures to *PSP*. The colored arrows mark the positions of the small transients in the images.

imagery offers a unique opportunity to track bright features continuously out to *PSP*; *PSP* was located at $PA = 265^\circ$ (i.e., between the two PAs labeled in the Figure 7). There is a constant ejection of blobs near the equatorial plane throughout the interval of interest. Most of the outflows seem to have a width lower than 15° and a speed of around 350 km s^{-1} . The ejection that extends most in PA (30°) during that time interval was imaged by HI1 around 21:29 UT on April 8 (see Figure 7 bottom panel). This blob exhibits V-shape structures and could consist of helical magnetic fields. The central axis feature propagates along $PA = 270^\circ$ and, as we shall see, *PSP* could have been impacted by its southern edge.

5. Tracing Density Structures from *PSP* Back to the Sun

The representation of white-light imagery in the form of time–elongation (or time–height) maps provides a powerful way to track the evolution of coronal structures moving through the optically thin solar atmosphere. These maps, traditionally called

J-maps, were first produced with LASCO C2/C3 images (Sheeley et al. 1999) and were subsequently adapted to *STEREO* COR and HI1 images (Sheeley et al. 2008; Davies et al. 2009). J-maps are constructed by extracting strips along a fixed PA from a sequence of coronagraph and/or heliospheric images. The extracted strips are plotted vertically as a function of time to generate an elongation versus time map. J-maps based on observations from near 1 au are typically built from running-difference images to minimize the contribution of the F-corona and to highlight faint propagating features.

Figure 8 presents such a J-map, derived from COR2A and HI1A images taken between 2019 April 6 and 11, along $PA = 265^\circ$. This PA was chosen to track features directed toward *PSP*'s position. Because white-light images are integrated along the line of sight, features directed along *PSP*'s PA are not necessarily directed toward *PSP*. COR2A observations extend out to an elongation of approximately 4° , while HI1 observations extend $\sim 4^\circ$ – 24° . From April 6 to 11, *PSP* was at an elongation (as viewed from *STA*) that varied from 9.9° to 11° .

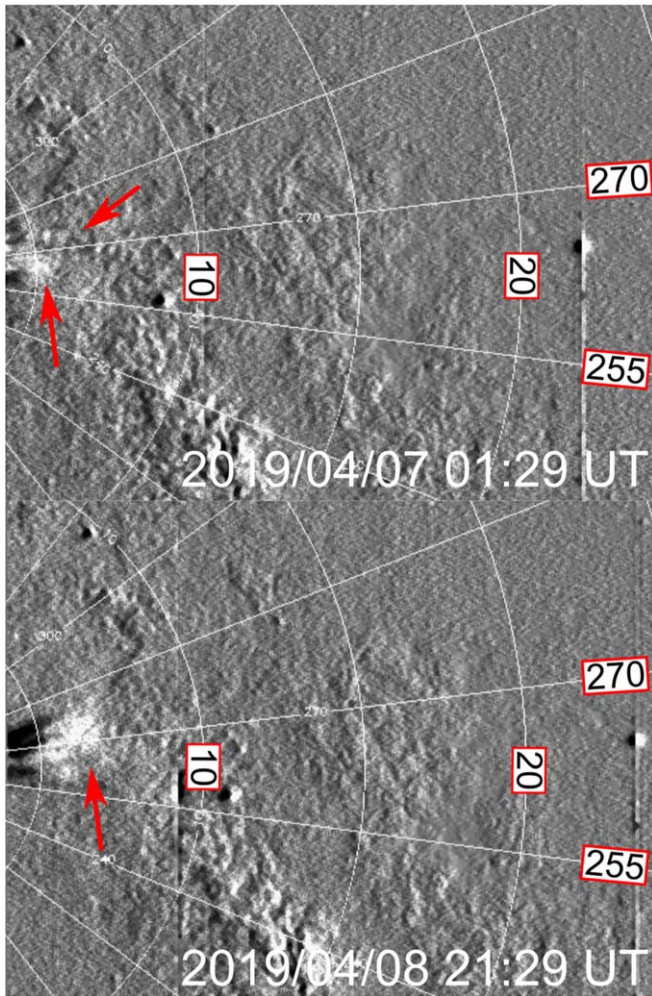


Figure 7. Two running-difference images from HI1A showing the bright features tracked to *PSP*. *PSP* is situated at a PA of 265° and near the 10° elongation mark at the time. The colored arrows mark the positions of the small transients in the images.

The J-map shown in Figure 8 covers the entire field of view of COR2A and about half of HI1A’s field of view, extending out just beyond the maximum elongation reached by *PSP* during the interval of interest (11°).

The J-map confirms that, during this time interval, a profusion of density structures erupted from the corona along the PA of *PSP*. This activity is particularly intense after April 7 (tick label 4/7). As can be seen in Figures 6 and 7, a significant burst of small eruptions occurs between 12UT on April 7 and 00UT on April 8. The shape of the tracks in the J-map shows that the density structures accelerate in the coronagraph field of view and then maintain a more constant progression through the inner part of the HI1A field of view, all the way to *PSP*.

In order to connect *PSP* measurements of sudden density changes with the inclined tracks seen in the J-maps, we plot in panels (a) and (b) of Figure 8, respectively, the radial speed and density of the solar wind plasma measured in situ by *PSP*. We mark some of the most notable density variations measured by *PSP* during that time interval with vertical dashed lines. For each impact, we know the measured radial speed of the density structure (V_r), the heliocentric radial distance of *PSP* (r_p), and the longitudinal separation between *STA* and *PSP* (β). The

latter changed from 68° to 124° during the interval spanned by the J-map. We then used the approach of Rouillard et al. (2010b) to compute the apparent elongation variation ($\alpha(t)$) that each density feature would show in the J-map if moving radially outwards at a constant speed of V_r :

$$\tan[\alpha(t)] = \frac{V_r t \sin(\beta)}{r_A - V_r t \cos(\beta)}, \quad (1)$$

where time t runs backwards from the time of impact at *PSP* and r_A is the radial distance of *STA*. We assume that β remains constant during the propagation of each structure—in other words, that *STA*’s longitude remains constant and that the radially outflowing features do not corotate with the Sun but, instead, moved in a purely heliocentric radial direction. *SPC* has detected a significant tangential component of the plasma velocity at its two first perihelia (Kasper et al. 2019/this volume). Any effect of plasma motion on the shape of the determined tracks is left to be investigated in a future study.

Nearly all of the density structures detected by *PSP* in situ have an apparent track that matches an observed track in the *STA* J-map. The varying inclination of the reconstructed tracks in the J-map is related to the corotation of the plasma source at the Sun. The density structures are expelled closer to the observer at the start of the interval than toward the end of the time interval. By visual inspection, we find that the best match between the observed and traced tracks occurs after April 7. Before this time, the connection of the in situ and J-maps tracks is more ambiguous; this is likely related to the positions of *PSP* with respect to the *STA* plane of the sky (and also the Thomson sphere).

We are able to relate the times of large density peaks measured by *PSP* on April 7 19:30 UT and April 9 04:10 UT to major bursts of bright tracks observed by HI near the elongation of *PSP*, which can be traced back into the COR2A field of view. These episodes of large density increases, as measured by *SPC*, contain sequences of smaller density peaks separated by around 90–120 minutes. They are clearly reflected as additional narrower tracks in the J-map. They are shown in Figures 8(a) and (b) by dashed vertical lines. Such density structures were noticed in past in situ measurements taken near 1 au (Viall et al. 2008), in *Helios* data between 0.3 and 0.6 au (Di Matteo et al. 2019), and separately in the spectral analysis of COR2A imagery (Viall & Vourlidas 2015). Combined *STA* and *PSP* observations allow, for the first time, investigation of the origin of individual features.

As a further check, we have analyzed the 3D trajectory of the density peaks using data from the full SECCHI field of view that extends out to 74° in elongation (corresponding to the outer edge of the HI2A field of view near the ecliptic plane). Over the time interval of interest here (April 6–12), most features completely fade as they near the outer edge of the HI1 field of view/inner edge of the HI2 field of view; this is expected for features that propagate in or near *STA*’s plane of the sky. A trajectory analysis of these tracks using the fixed-phi technique (Equation (1)) that assumes plasma parcels move radially outwards at constant speed (e.g., Rouillard et al. 2008, 2009) yields values of β ranging between 70° and 100° , confirming that the features are expelled close to the plane of the sky during that time interval.

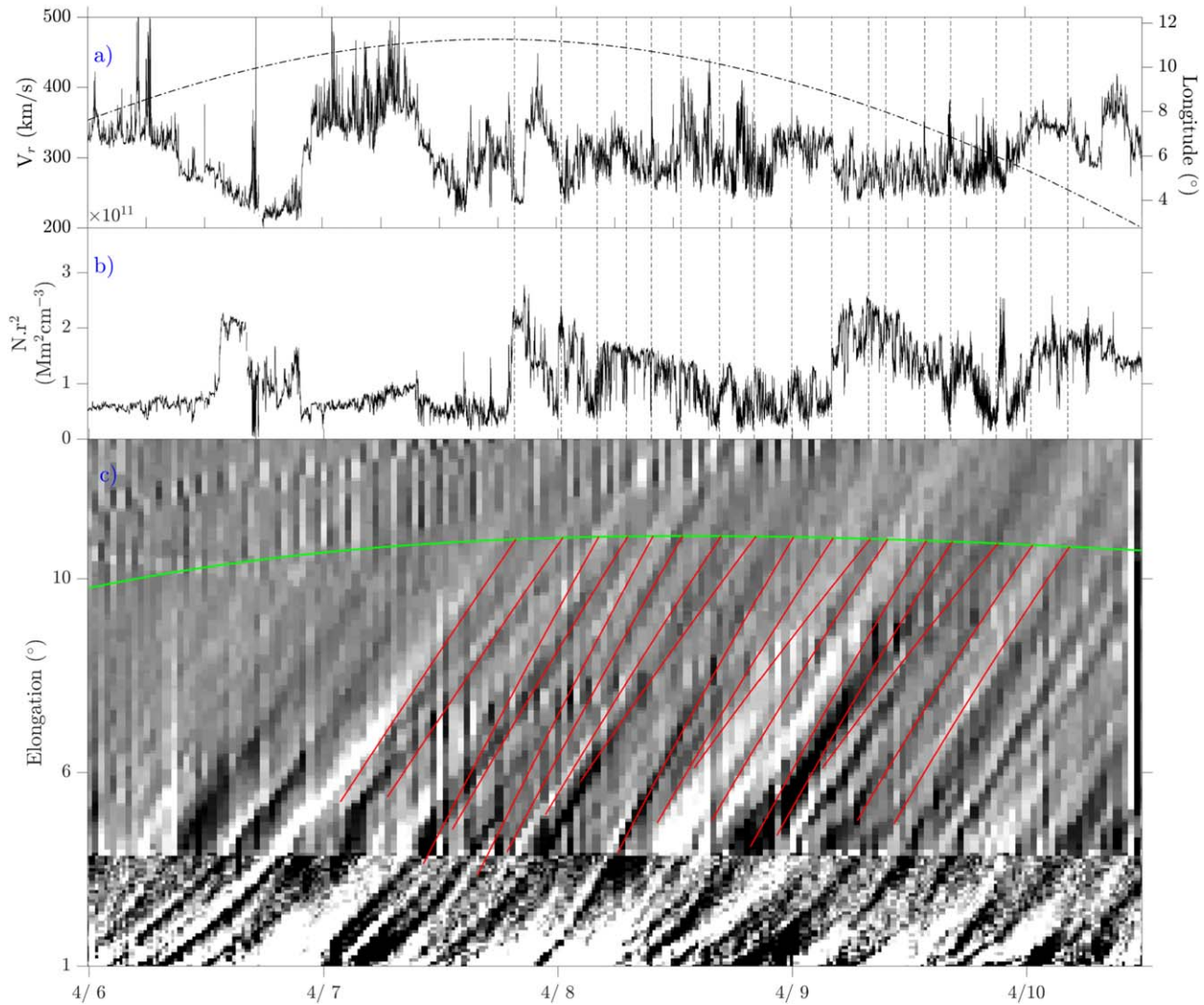


Figure 8. Panels (a) and (b): the radial component of the solar wind speed and the density measured by SPC. The Carrington longitude of *PSP* is shown as a dashed-dotted line in panel (a). The vertical dashed lines plotted in both panels (a) and (b) mark the onset of noticeable density variations. Panel (c): a J-map constructed from COR2A and H11A images. The green curve shows the elongation variation of *PSP* during this time interval. The red curves are the time–elongation profiles of density structures marked by the vertical bars in panels (b), assuming each of the structure propagates from the Sun to *PSP* at the speed measured in situ (panel (a)).

6. Discussion

The source regions of the different components of the slow solar wind are still debated. We know that the densest regions of the upper corona are associated with the bright coronal rays that emanate from helmet streamers. They have been long thought to generate the densest slow solar wind measured in situ, in particular hosting the source region of HPS that engulfs the HCS. Recent studies revisiting past data have argued that the slowest and densest solar wind measured in situ results from a magnetic connection in the vicinity of the coronal neutral line (Sanchez-Diaz et al. 2016).

In this paper, we have combined multipoint imagery taken by *STEREO* and *SOHO* with the unprecedented in situ and remote-sensing observations made by *PSP* of the nascent slow solar wind.

1. We make the first direct association between streamer rays and the dense solar wind measured in situ by *PSP*.
2. We show that, as it moved to its southernmost heliographic latitudes near perihelion, *PSP* briefly exited

the streamer rays. It then entered a region that appeared precisely when SPC measured more tenuous and less variable plasma measured in situ.

3. We demonstrate that *PSP* remained on one side of the streamer belt around perihelion.
4. We reveal a direct association between small white-light transients and density variations measured in situ by *PSP* on timescales of tens of hours down to tens of minutes.
5. We show that the white-light transients tracked to *PSP* along the edge of the streamers contain many switch-backs associated with high densities.

These connections provide further context for interpreting the findings of Bale et al. (2019) and Kasper et al. (2019). Because *PSP* remained on one side of the streamer, the HCS was not measured during this period and remained in one polarity sector.

In addition, *PSP* did not cross clear magnetic flux ropes that are expelled from the more central regions of the streamer. The last two decades of research have shown that streamer rays are continually perturbed by bursts of transient outflows

(Sheeley et al. 1997; Sheeley & Rouillard 2010; Rouillard et al. 2011) released quasiperiodically from the top of helmet streamers. Multipoint imagery suggests they are formed by magnetic reconnection near $3\text{--}5 R_{\odot}$ (Sanchez-Diaz et al. 2017a, 2017b). These “blobs” normally disappear rapidly in the field of view of HI due to the drop in density associated with their expansion (e.g., Rouillard et al. 2008). On occasion, these very slow transients get swept up by high-speed streams, thereby maintaining their high densities all the way to 1 au. The largest, and hence more massive, of these blobs have been tracked all the way to in situ spacecraft and have also been associated with the passage of helical magnetic fields (Rouillard et al. 2010b, 2010a). These flux ropes are measured in situ in the HCS (Rouillard et al. 2009, 2011) between two sector boundaries.

Poirier et al. (2020) show that the zoomed-in view of streamer rays provided by WISPR enables a mapping of the small-scale morphology of streamers. This includes the densest part of the streamers where the HPS originates, this very high-density region that engulfs the HCS (Winterhalter et al. 1994). We have used a WISPR Carrington map (Figure 5) to compare the location of *PSP* with this HPS at the start of the encounter (March 23–27); even then, *PSP* remained several degrees south of the likely location of the HCS (orange arrows in Figure 5). Individual WISPR images also show that flux rope structures were ejected continually northwards of *PSP*. Therefore, the core of these flux rope structures were not expected to impact the *PSP* spacecraft during that time interval.

Instead of a clean flux rope crossing, *PSP* measured local reversals of the magnetic field direction that were not associated with 180° changes in the pitch angle of suprathermal electrons. These structures are interpreted in Bale et al. (2019) and Kasper et al. (2019) as folds in the magnetic fields that are often associated with density increases. They suggest that these higher densities should be detected in coronal and heliospheric imaging. The present study confirms this and connects the variable outflows from the streamers with strong bursts of “switchbacks.”

Comparing Figure 4 with Figure 3, we find evidence that these switchbacks have different properties inside and outside streamer flows (Figure 4). The switchbacks in streamer flows tend to occur in bursts or clumps lasting several hours with sustained and significant changes in plasma density. Switchbacks originating from outside streamer stalks, likely from deeper inside coronal holes, are shorter lived and more numerous. These differences will be investigated further in an upcoming publication.

The present studies provides new clues to interpret the origin of the highly structured flows revealed by the analysis of deep-field *STEREO*/COR2 observations (DeForest et al. 2018). The latter study predicted that *PSP* would encounter “strong, sharp variations in plasma density, by as much as an order of magnitude on timescales of 10 minutes or less.” We have shown that the strong density variations are measured in situ by *PSP* mainly inside streamer flows (Figure 4). We conclude that the strong density variations revealed by *STEREO* are likely to originate inside and on the edges of streamer rays. The apparently ubiquitous nature of the density structures revealed by the analysis of DeForest et al. (2018) could be related to the presence of streamer rays at all PAs around the Sun. This would be expected at times of elevated solar activity that typically forces large excursions of the coronal neutral line and its associated helmet streamer. We also conclude that the

structures imaged by DeForest et al. (2018) are likely to transport kinks and reversals in the magnetic field lines.

Magnetic reconnection (e.g., Owens et al. 2018), perhaps from chromospheric/coronal jets (e.g., Horbury et al. 2018), and Kelvin–Helmholtz instabilities (e.g., Suess et al. 2009) have been invoked as important physical mechanisms occurring at the interface between open and closed field lines, where the plasma escaping along open magnetic field lines meets the more static loop plasma. Both mechanisms could, in principle, produce folds in the magnetic field and plasma mixing at the boundary layers.

If we assume that switchbacks are formed by magnetic reconnection between open and closed magnetic field lines, a possible explanation for their different properties inside and outside streamer flows could reside in the size of the loops involved in the reconnection process. Streamer flows form above streamers where the largest coronal loops are typically adjacent to open magnetic field lines. These large loops are associated with dense plasma seen as bright helmet streamers in white-light images. In contrast, the smaller switchbacks measured just outside streamer flows could form in smaller loops lower in the corona. This idea could be tested in a future study by using composition data such as alpha to proton ratio changes associated with trains of density structures (Viall et al. 2009). Future measurements of heavier ions by the *Solar Orbiter* will be invaluable to investigate whether switchbacks inside and outside streamer flows contain different proportions of elements with low first-ionization potential (Laming et al. 2019).

7. Conclusion

The *PSP* mission is providing an unprecedented opportunity to connect solar winds with their source regions in the corona. This article has demonstrated the power of using multipoint and multi-instrument studies to study the sources of the slow solar wind. In doing so, we have made a clear connection between density variations expelled along the edges of streamers and density structures measured in situ, providing new clues on the origin and structure of the slow solar wind. In future studies, we will attempt to link the magnetic properties of the small-scale transients with physical processes occurring in the corona using a combination of modeling and remote-sensing and in situ observations.

A better understanding of the dynamic outflows of streamers is important for other areas of solar physics. This region must host magnetic loop emergence and the periodic disconnection of open magnetic fields implicated in the long-term evolution of the open flux. The presence of switchbacks in the magnetic field was suggested in past studies of the total solar magnetic flux derived from in situ measurements (Lockwood et al. 2009a). Folds in the magnetic field were invoked as a source of the apparent increase of the total open flux (the flux excess effect) with heliocentric radial distance (Lockwood et al. 2009b). Recent studies have also found evidence that the highest energy particles could be accelerated when strong shocks reach the tip of streamers (e.g., Rouillard et al. 2016; Kouloumvakos et al. 2019). The next decade of research with *PSP* and the *Solar Orbiter* promises to be rich in new discoveries on streamer flows.

The IRAP team acknowledges support from the French space agency (Centre National des Etudes Spatiales, CNES; <https://cnes.fr/fr>) that funds the plasma physics data center (Centre de Données de la Physique des Plasmas, CDPP; <http://www.cdpp.eu/>), the Multi Experiment Data & Operation Center (MEDOC; <https://idoc.ias.u-psud.fr/MEDOC>), and the

space weather team in Toulouse (Solar-Terrestrial Observations and Modeling Service, STORMS; <https://stormsweb.irap.omp.eu/>). This includes funding for the data mining tools AMDA (<http://amda.cdpp.eu/>) and CLWEB (<http://clweb.irap.omp.eu/>), and the propagation tool (<http://propagationtool.cdpp.eu/>). A.K. and Y. W. acknowledge financial support from the ANR project SLOW_SOURCE (ANR-18-ERC1-0006-01), COROSHOCK (ANR-17-CE31-0006-01), and FP7 HELCATS project <https://www.helcats-fp7.eu/> under the FP7 EU contract number 606692. The work of A.P.R., N.P., L.G., V.R., and P.L. was funded by the ERC SLOW_SOURCE project (SLOW_SOURCE—DLV-819189). The work of A.V., R.A.H., and G.S.g was supported by the PSP/WISPR project. N.M.V. is supported by the NASA Heliophysics Internal Scientist Funding Model. We thank the PSP, STEREO/SECCHI, and SOHO/LASCO teams.

Facilities: Solar and Heliospheric Observatory, Solar-Terrestrial Relations Observatory.

ORCID iDs

Alexis P. Rouillard  <https://orcid.org/0000-0003-4039-5767>
 Angelos Vourlidas  <https://orcid.org/0000-0002-8164-5948>
 Justin Kasper  <https://orcid.org/0000-0002-7077-930X>
 Stuart Bale  <https://orcid.org/0000-0002-1989-3596>
 Benoit Lavraud  <https://orcid.org/0000-0001-6807-8494>
 Russell A. Howard  <https://orcid.org/0000-0001-9027-8249>
 Guillermo Stenborg  <https://orcid.org/0000-0001-8480-947X>
 Michael Stevens  <https://orcid.org/0000-0002-7728-0085>
 Nicolas Poirier  <https://orcid.org/0000-0002-1814-4673>
 Aleida K. Higginson  <https://orcid.org/0000-0003-1380-8722>
 Nicholeen M. Viall  <https://orcid.org/0000-0003-1692-1704>
 Kelly Korreck  <https://orcid.org/0000-0001-6095-2490>
 Rui F. Pinto  <https://orcid.org/0000-0001-8247-7168>
 Victor Réville  <https://orcid.org/0000-0002-2916-3837>
 Kévin Dalmasse  <https://orcid.org/0000-0001-8929-4006>
 Anthony W. Case  <https://orcid.org/0000-0002-3520-4041>
 Jasper S. Halekas  <https://orcid.org/0000-0001-5258-6128>
 Robert J. MacDowall  <https://orcid.org/0000-0003-3112-4201>
 D. Malaspina  <https://orcid.org/0000-0003-1191-1558>
 M. Pulupa  <https://orcid.org/0000-0002-1573-7457>
 T. Dudok de Witt  <https://orcid.org/0000-0002-4401-0943>

References

- Baker, D., Rouillard, A. P., van Driel-Gesztelyi, L., et al. 2009, *AnGeo*, **27**, 3883
 Bale, S., Badman, S. T., Bonnell, J. W., et al. 2019, *Natur*, **576**, 237
 Bale, S. D., Goetz, K., Harvey, P. R., et al. 2016, *SSRv*, **204**, 49
 Bame, S. J., Asbridge, J. R., Feldman, W. C., et al. 1976, *ApJ*, **207**, 977
 Bewsher, D., Brown, D. S., & Eyles, C. J. 2012, *SoPh*, **276**, 491
 Brueckner, G. E., Howard, R. A., Koomen, M. J., et al. 1995, *SoPh*, **162**, 357
 Case, A. W., Kasper, J. C., Stevens, M. L., et al. 2020, *ApJS*, doi:10.3847/1538-4365/ab5a7b
 Culhane, J. L., Brooks, D. H., van Driel-Gesztelyi, L., et al. 2014, *SoPh*, **289**, 3799
 Davies, J. A., Harrison, R. A., Rouillard, A. P., et al. 2009, *GeoRL*, **36**, L02102
 DeForest, C. E., Howard, R. A., Velli, M., et al. 2018, *ApJ*, **862**, 18
 Di Matteo, S., Viall, N. M., Kepko, L., et al. 2019, *JGRA*, **124**, 837
 Druckmüller, M., Habbal, S. R., & Morgan, H. 2014, *ApJ*, **785**, 14
 Eyles, C. J., Harrison, R. A., Davis, C. J., et al. 2009, *Natur*, **454**, 387
 Horbury, T. S., Matteini, L., Stansby, D., et al. 2018, *MNRAS*, **478**, 1980
 Howard, R. A., Moses, J. D., Vourlidas, A., et al. 2008, *SSRv*, **136**, 67
 Kasper, J. C., Abiad, R., Austin, G., et al. 2016, *SSRv*, **204**, 131
 Kasper, J. C., Bale, S. D., Belcher, J. W., et al. 2019, *SoPh*, **254**, 228
 Kepko, L., Viall, N. M., Antiochos, S. K., et al. 2016, *GeoRL*, **43**, 4089
 Kojima, M., Fujiki, K., Ohmi, T., et al. 1999, *JGR*, **104**, L6993
 Kouloumvakos, A., Rouillard, A. P., Wu, Y., et al. 2019, *ApJ*, **876**, 80
 Krieger, A. S., Timothy, A. F., & Roelof, E. C. 1973, *SoPh*, **29**, 505
 Laming, J. M., Vourlidas, A., Korendyke, C., et al. 2019, *ApJ*, **879**, 124
 Levine, R. H., Altschuler, M. D., & Harvey, J. W. 1977, *JGR*, **82**, 1061
 Linker, J. A., Mikić, Z., Biesecker, D. A., et al. 1999, *JGR*, **104**, 9809
 Lockwood, M., Owens, M., & Rouillard, A. P. 2009a, *JGR*, **114**, A11103
 Lockwood, M., Owens, M., & Rouillard, A. P. 2009b, *JGR*, **114**, A11104
 Owens, M. J., Lockwood, M., Barnard, L. A., et al. 2018, *ApJL*, **868**, L14
 Pinto, R. F., & Rouillard, A. P. 2017, *ApJ*, **838**, 89
 Poirier, N., Kouloumvakos, A., Rouillard, A. P., et al. 2020, *ApJS*, doi:10.3847/1538-4365/ab6324
 Rouillard, A. P., Davies, J. A., Forsyth, R. J., et al. 2008, *GeoRL*, **35**, L10110
 Rouillard, A. P., Davies, J. A., Lavraud, B., et al. 2010a, *JGRA*, **115**, A04103
 Rouillard, A. P., Lavraud, B., Génot, V., et al. 2017, *P&SS*, **147**, 61
 Rouillard, A. P., Lavraud, B., Sheeley, N. R., et al. 2010b, *ApJ*, **719**, 1385
 Rouillard, A. P., Plotnikov, I., Pinto, R. F., et al. 2016, *ApJ*, **833**, 45
 Rouillard, A. P., Savani, N. P., Davies, J. A., et al. 2009, *SoPh*, **256**, 307
 Rouillard, A. P., Sheeley, N. R., Cooper, T. J., et al. 2011, *ApJ*, **734**, 7
 Sanchez-Diaz, E., Rouillard, A. P., Davies, J. A., et al. 2017a, *ApJ*, **851**, 32
 Sanchez-Diaz, E., Rouillard, A. P., Davies, J. A., et al. 2017b, *ApJL*, **835**, L7
 Sanchez-Diaz, E., Rouillard, A. P., Lavraud, B., et al. 2016, *JGRA*, **121**, 2830
 Sheeley, N. R., Herbst, A. D., Palatchi, C. A., et al. 2008, *ApJ*, **675**, 853
 Sheeley, N. R., Lee, D. D., Casto, K. P., et al. 2009, *ApJ*, **694**, 1471
 Sheeley, N. R., & Rouillard, A. P. 2010, *ApJ*, **715**, 300
 Sheeley, N. R., Walters, J. H., Wang, Y.-M., et al. 1999, *ApJ*, **104**, 24739
 Sheeley, N. R., Wang, Y.-M., Hawley, S. H., et al. 1997, *ApJ*, **484**, 472
 Stenborg, G., Howard, R. A., & Stauffer, J. R. 2018, *ApJ*, **862**, 168
 Suess, S. T., Ko, Y.-K., von Steiger, R., & Moore, R. L. 2009, *JGR*, **114**, A04103
 Tappin, S. J., Eyles, C. J., & Davies, J. A. 2015, *SoPh*, **290**, 2143
 van der Holst, B., Manchester, W. B., IV, Frazin, R. A., et al. 2010, *ApJ*, **725**, 1373
 van Driel-Gesztelyi, L., Culhane, J. L., Baker, D., et al. 2012, *SoPh*, **281**, 237
 Viall, N. M., Kepko, L., & Spence, H. E. 2008, *JGR*, **113**, A07101
 Viall, N. M., Spence, H. E., & Kasper, J. 2009, *GeoRL*, **36**, L23102
 Viall, N. M., & Vourlidas, A. 2015, *ApJ*, **807**, 176
 Vourlidas, A., & Howard, R. A. 2006, *ApJ*, **642**, 1216
 Vourlidas, A., Howard, R. A., Plunkett, S. P., et al. 2016, *SSRv*, **204**, 83
 Wang, Y. M. 1994, *ApJ*, **437**, L67
 Wang, Y.-M., Sheeley, N. R., & Rich, N. B. 2007, *ApJ*, **658**, 1340
 Winterhalter, D., Smith, E. J., Burton, M. E., et al. 1994, *JGR*, **99**, 6667
 Xu, F., & Borovsky, J. E. 2015, *JGRA*, **120**, 70